Intramolecular Dynamics in the Photofragmentation of Initially Vibrationally Excited CH 2 Cl 2 †

ARTICLE *in* THE JOURNAL OF PHYSICAL CHEMISTRY A · SEPTEMBER 2004

Impact Factor: 2.69 · DOI: 10.1021/jp049217w

4 AUTHORS, INCLUDING:

S. Rosenwaks
Ben-Gurion University of the Negev
257 PUBLICATIONS **3,471** CITATIONS

SEE PROFILE

Ilana Bar
Ben-Gurion University of the Negev
172 PUBLICATIONS **2,254** CITATIONS

SEE PROFILE

Intramolecular Dynamics in the Photofragmentation of Initially Vibrationally Excited CH_2Cl_2†

Ran Marom, Amir Golan, Salman Rosenwaks,‡ and Ilana Bar*,§

Department of Physics, Ben-Gurion University of the Negev, Beer-Sheva 84105, Israel

Received: February 20, 2004; In Final Form: April 8, 2004

The intramolecular dynamics of dichloromethane was studied by applying vibrationally mediated photodissociation and photoacoustic spectroscopy. The parent species were initially excited to the second, third, and fourth C−H stretch overtone regions and subsequently photodissociated by ∼235 nm photons that also tagged the ground, $Cl(^2P_{3/2})$ [Cl], and spin−orbit-excited, $Cl(^2P_{1/2})$ [Cl*], state photofragments via resonantly enhanced multiphoton ionization. The Cl and Cl* action spectra revealed enhancement of their yield as a result of rovibrational excitation with a Cl*/Cl ratio of about 1/2. The action and photoacoustic spectra manifested a multiple-peak structure, which in terms of normal- and local-mode models is shown to be related to overtones of C−H stretches or combination bands of C−H stretches and bends. The measured time-of-flight profiles together with the determined Cl*/Cl branching ratios suggest fast dissociation and involvement of upper states of A′ and A″ symmetry, mixing via curve crossing and releasing both Cl and Cl*. The determined Cl*/Cl ratios in photodissociation of vibrationally excited CH_2Cl_2 are higher than those obtained previously in 193 nm photodissociation of the vibrationless ground state, implying higher nonadiabaticity for the former.

Introduction

The study of halogen-containing molecules gained considerable interest during the last three decades due to their atmospheric importance and interesting photodissociation dynamics. The atmospheric concern is related to the production of active halogen atoms and radicals in the UV dissociation of haloalkanes, playing a major role in ozone depletion from the earth's ozone layer.[1] The interest in the fragmentation pattern rose due to the inherent complexity where halogen atoms, which are open shell atoms, are produced.[2] Indeed, theoretical and experimental studies on mono- and dihaloalkanes revealed the release of both ground, $X(^2P_{3/2})$ [X], and spin−orbit-excited, $X(^2P_{1/2})$ [X*], state halogen atoms as a result of C−X (X = Cl, Br, and I) bond cleavage. By determining the velocity distribution of the photofragments together with their anisotropy parameters and branching ratios, information regarding the dynamics on the excited potential energy surfaces (PESs) could be obtained. [3−20] Generally, it is accepted that the photodissociation process entails more than one excited PES and is accompanied by nonadiabatic curve crossing dynamics during the photofragmentation.

Recently, exploration of the effect of initial state preparation on the yield of ground and spin−orbit-excited halogen atoms turned out to be of much interest. For example, in CH_3I, which serves as a benchmark for understanding polyatomic fragmentation patterns, it was shown that the I*/I product branching measures the behavior of the molecule through the conical intersection of the $^1Q_1$ and $^3Q_0$ PESs.[4,5,9,12] Particularly, it was predicted that the nonadiabatic transitions from $^3Q_0$ to $^1Q_1$ can be enhanced by excitation of parent bending,[5] or methyl rocking[4] due to the destruction of the C_{3v} symmetry. Butler and co-workers[21] observed a change in the branching between the CF_3 + I and I* product channels when hot rather than cold CF_3I was photodissociated at 248.5 nm. An increase in the branching ratio into Cl* was also observed by Lambert and Dagdigian[22] in vibrationally mediated photodissociation (VMP)[23,24] of CH_3Cl and CHD_2Cl pre-excited to the fourth overtone of the C−H stretch, with a larger increase in the former. Furthermore, we encountered alteration of the branching ratio in the VMP of CH_3CF_2Cl and CH_3CFCl_2, as compared to the almost isoenergetic vibrationless ground-state photodissociation.[25]

The exploration of vibrationally excited molecules with CH stretch chromophores is also of interest since it provides one of the means for elucidating intramolecular vibrational energy redistribution (IVR).[26−28] The observation of vibrational eigenstates, splittings, and relative intensities in frequency-domain experiments and their analysis allow couplings that are involved in energy flow to be revealed and the time scales for energy redistribution of the nonstationary states to be inferred. Consequently, insight into the behavior of nonstationary states that would change in time if they were prepared under coherent excitation is obtained.

In a preliminary study we have shown that dissociation of dichloromethane, CH_2Cl_2, pre-excited to the second C−H stretch overtone also affects the branching into Cl and Cl*.[29] Here we further investigate the impact of initial vibrational excitation in the region of the second to fourth C−H stretch overtones. Jet-cooled Cl and Cl* action and photoacoustic (PA) spectra show a multiple-peak structure, which in terms of normal-mode (NM) and local-mode (LM) models is shown to be related to C−H stretch overtones or combinations of C−H stretches and bends, manifesting the time scale for energy redistribution. The Cl*/Cl branching ratios and the time-of-arrival profiles of ^{35}Cl and ^{35}Cl* characterize the primary decay process and provide some insight into the intramolecular dynamics on the excited PESs.

† Part of the special issue "Richard Bersohn Memorial Issue".

* To whom correspondence should be addressed. E-mail: ibar@bgu.ac.il.

‡ The Helen and Sanford Diller Family Chair in Chemical Physics.

§ Also at The Institutes for Applied Research, Ben-Gurion University of the Negev.

10.1021/jp049217w CCC: $27.50
Published on Web 05/27/2004

Experiment

The experiments were performed with the previously described setup,[25,29,30] including a home-built time-of-flight mass spectrometer (TOFMS) and two tunable lasers, one for vibrational excitation and the second for photolysis of CH_2Cl_2 and probing of the Cl and Cl* photofragments. The CH_2Cl_2 sample (99.9+% purity) was thoroughly degassed at reduced temperatures and then mixed with Ar to provide a ~10% mixture at a total pressure of ~760 Torr. The molecular beam was expanded into the ionization chamber perpendicularly to the TOFMS axis and the laser beams (see below). The expansion was carried out through a nozzle−skimmer arrangement, to typical pressures of $\sim 5 \times 10^{-6}$ Torr. Under these conditions the beam was characterized by a predominant rotational temperature of ~10 K and a vibrational temperature of <100 K. These temperatures were estimated from VMP studies of propyne-d_3, carried out under similar conditions.[31]

The molecular beam was intersected by a near-infrared (NIR) laser beam around 1151, 880, and 722 nm from the idler of an optical parametric oscillator, which was pumped by the third harmonic output of a Nd:YAG laser. This laser beam with energies of ~10, 13, and 30 mJ, respectively, and a bandwidth of ~0.08 cm^{-1} vibrationally excited the parent molecule in the region of three, four, and five C−H stretch quanta. Following the excitation pulse, after a delay of ~10 ns, the excited CH_2Cl_2 molecules were photodissociated by a counterpropagating UV beam (~130 μJ) from a frequency-doubled tunable dye laser (~0.4 cm^{-1}) pumped by the third harmonic of a second Nd:YAG. The wavelength of this beam was chosen to match the two-photon transitions of Cl ($4p\ ^2D_{3/2} \leftarrow 3p\ ^2P_{3/2}$) at 235.336 nm and Cl* ($4p\ ^2P_{1/2} \leftarrow 3p\ ^2P_{1/2}$) at 235.205 nm to also detect the Cl and Cl* photofragments, respectively, by (2 + 1) resonantly enhanced multiphoton ionization (REMPI). The NIR beam was focused with a 15 cm focal length (fl) lens, while the photolysis/probe (UV) beam was focused with a 30 cm fl lens. The CH_2Cl_2 molecules were photolyzed efficiently only when the molecules were pre-excited to the corresponding overtone, due to the very low absorption cross section of vibrationless ground-state molecules at ~235 nm (1.16×10^{-22} cm^2).[32] The obtained enhancements for the highest peak in each range were about 200, 40, and 5 for the regions of the second, third, and fourth C−H overtones, respectively.

Ions formed via REMPI in the focal volume were subject to continuously biased extraction, two acceleration stages, two pairs of orthogonal deflection plates, and an einzel lens. The ions then entered the field-free drift region (55 cm long) and were detected by a microsphere plate (MSP). The MSP output was amplified and fed into a digital oscilloscope and a boxcar integrator where wavelength-dependent ion signals of ^{35}Cl, ^{37}Cl, $^{35}Cl^*$, and $^{37}Cl^*$ were captured and processed by a computer. The signals of masses 35 and 37 were monitored simultaneously by two independent boxcar channels, taking advantage of the mass resolution of the TOFMS. Action spectra measuring the yield of the released Cl and Cl* photofragments as a function of the NIR wavelength laser were monitored by setting the UV laser on the corresponding chlorine transitions. Each data point in the ensuing spectra was an average of 30 pulses. In addition, Doppler profiles were measured to determine the Cl*/Cl branching ratios, by fixing the NIR laser on the most intense peak (see below) and scanning the UV laser across the Cl and Cl* transitions. The profiles were well fitted by Gaussians, and their integrated areas were used to calculate the Cl*/Cl ratio once the scaling factor of the above-mentioned transitions was accounted for.[33] Furthermore, time-of-arrival profiles of the ^{35}Cl and $^{35}Cl^*$ resulting from 5000 shots were recorded, while the NIR laser was set on the most intense peak and the UV laser on the Cl and Cl* transitions, with the digital oscilloscope and stored for later analysis. The time-of-arrival profiles were measured under space focusing conditions at two different geometries, vertical (UV laser polarization perpendicular to the TOF axis) and horizontal (UV laser polarization parallel to the TOF axis). The effects of the apparatus on the TOF were previously determined,[30] allowing calibration of the electric field strength, E, in the ionization region. The profiles were modeled using the forward convolution method,[30] accounting for the field strength, the finite time response of the apparatus (a Gaussian with a 20 ns full width at half-maximum), and the Doppler selection by the finite bandwidth of the probe laser (0.3 cm^{-1} at the one-photon wavenumber). Modeling of these profiles allowed extraction of the kinetic energy distributions and the anisotropy parameters.

Simultaneously with the action spectra, the room-temperature vibrational absorption spectrum was monitored by PA spectroscopy. This was achieved by directing the residual of the NIR beam, after passing through the TOFMS, to a dichroic mirror which reflected it into an auxiliary PA cell. The wavelength was calibrated by monitoring the rovibrational overtone spectra of water and determining the wavelength according to the positions of the water absorption lines taken from the HITRAN database.[34]

Results and Discussion

(a) Dynamics on the Ground-State PES. Figure 1 shows the room-temperature PA spectra and the Cl jet-cooled action spectra in the range of the second (panel a), third (panel b), and fourth (panel c) overtones of the C−H stretch of CH_2Cl_2. It is clearly seen that a multiple-peak structure appears in each range. However, by going from the second to the fourth C−H stretch overtone, the shapes change from well-defined envelopes to featureless peaks. Particularly, the central feature in the region of the second overtone shows a prominent Q-branch with well-defined P and R contours, which becomes less pronounced in the third overtone region and last washed out in the fourth overtone region.

Although the overtone spectra of CH_2Cl_2 were studied by several groups, a clear picture regarding the features observed in the different energetic regions was still missing.[35−38] This led us to analyze the spectra in terms of NM and LM models, where the former was used for the $\nu_{C-H} = 3$ region and the latter for the $\nu_{C-H} = 4$ and 5 regions, since thus the models could well match the features observed in all three regions. The NM model was previously successfully applied to CH_2Cl_2 and CD_2Cl_2 in the region below 6200 cm^{-1}.[35] Here it was extended to the 8700 cm^{-1} region by employing the fundamental frequencies (ν_1, ν_2, and ν_6) and their anharmonicity constants, x_{ij}, via the diagonal elements of the NM Hamiltonian matrix given by[35,39]

$$\langle \nu_1,\nu_2,\nu_6|H/hc|\nu_1,\nu_2,\nu_6\rangle = \nu_1\nu_1 + \nu_2\nu_2 + \nu_6\nu_6 + x_{11}\nu_1(\nu_1 - 1) + x_{22}\nu_2(\nu_2 - 1) + x_{66}\nu_6(\nu_6 - 1) + x_{12}\nu_1\nu_2 + x_{16}\nu_1\nu_6 + x_{26}\nu_2\nu_6 \quad (1)$$

and the off-diagonal coupling terms considering the Fermi resonance given by[35]

$$\langle \nu_1,\nu_2,\nu_6|H/hc|\nu_1-1,\nu_2+2,\nu_6\rangle = \frac{1}{2}k_{122}\left[\frac{\nu_1}{2}(\nu_2+1)(\nu_1+2)\right]^{1/2} \quad (2)$$

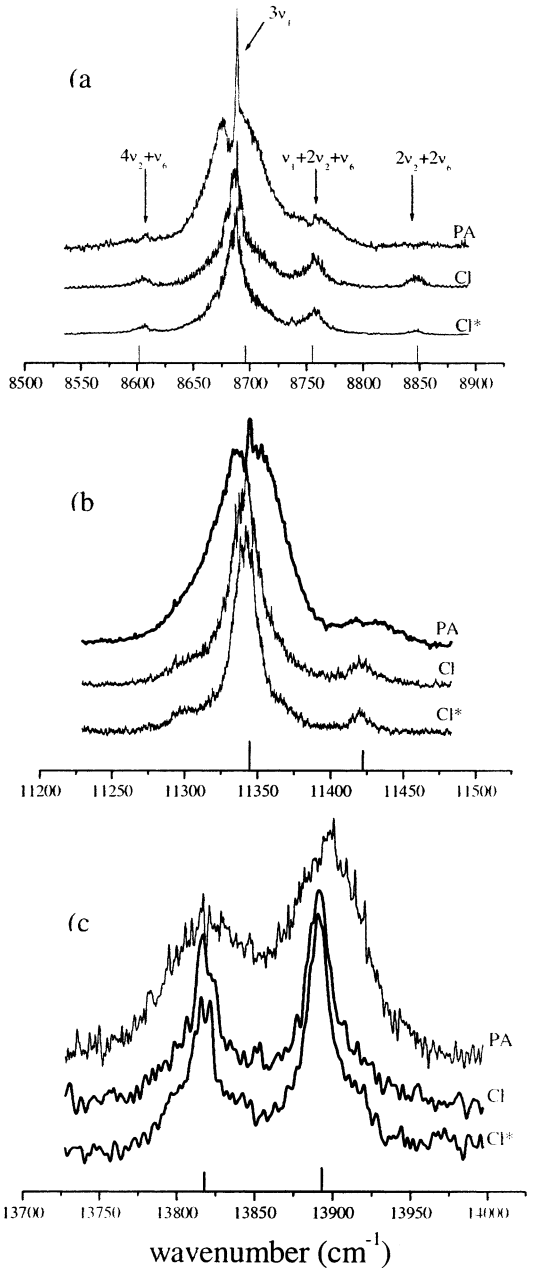

Figure 1. Vibrational overtone spectra of CH_2Cl_2 in the regions of the second (a), third (b), and fourth (c) overtones of the C−H stretch: room-temperature PA spectrum and jet-cooled action spectra of ^{35}Cl and ^{35}Cl*. The sticks below the spectra represent the calculated position in terms of NM (a) and LM models (b, c). The heights of the sticks in panels b and c represent the calculated contributions from the $\{\langle v,0,0|\}$ states,[44] which indicate the coupling of the C−H LM stretching states with the rest of the C−H stretch−bend manifold.

The values of Duncan et al.[35] were adopted for the C−H stretches, $\nu_1 = 2995.80\ cm^{-1}$ and $\nu_6 = 3055.0\ cm^{-1}$, for the C−H bending, $\nu_2 = 1435.0\ cm^{-1}$, for the anharmonicities, $x_{12} = -13.3$, $x_{16} = -119.0$, $x_{22} = -7.3$, $x_{26} = -23.1$, and $x_{66} = -19.5$, and for the resonance parameter, $k_{122} = 32.5\ cm^{-1}$. The initial value of x_{11} was $-43.0\ cm^{-1}$, and it was slightly adjusted to fit the positions of the bands appearing in the second C−H stretch overtone region and found to be $-45.4\ cm^{-1}$. It should be noted that this value did not alter significantly the calculated positions of the bands in the region of the first C−H stretch overtone and fundamental. The diagonalization of the matrix resulted in the eigenvalues marked by the sticks corresponding to the $4\nu_2 + \nu_6$, $3\nu_1$, $\nu_1 + 2\nu_2 + \nu_6$, and $2\nu_2 + 2\nu_6$ states (Figure 1a). This assignment agrees very well with that of Halonen[38] obtained with the curvilinear internal coordinate model.

The higher overtones were analyzed with the LM model, which treats the pair of C−H bonds in CH_2Cl_2 as independent anharmonic (Morse) diatomic oscillators, harmonically coupled to each other.[37,40,41] The diagonal elements of the LM Hamiltonian are[42]

$$\langle V|H/hc|V\rangle = \sum_i \left[\omega_{C-H}\left(n_i + \frac{1}{2}\right) + x_{C-H}\left(n_i + \frac{1}{2}\right)^2\right] \quad (3)$$

where ω_{C-H} is the LM harmonic vibration wavenumber, x_{C-H} is the anharmonicity, n_i is the quantum number in the ith C−H stretch, and $V = \sum_{i=1}^{2} n_i$. Also, the diagonal elements include additional terms due to a combination of the C−H stretch and bend, b, where $V = \sum_{i=1}^{2}(n_i + b/2)$, with the elements being $\delta_{C-H}(b + 1/2) + x_{bb}(b + 1/2)^2 + x_{sb}(b + 1/2)\sum_{i=1}^{2}(n_i + 1/2)$, where δ_{C-H} is the bend fundamental and x_{sb} and x_{bb} are the anharmonicities of the stretch−bend and bend−bend combinations, respectively. In addition, the interbond coupling yields off-diagonal matrix elements as[42]

$$\langle n_i,n_j|H/hc|n_i+1,n_j-1\rangle = \lambda^{HH}[(n_i + 1)n_j]^{1/2} \quad (4)$$

where λ^{HH} is the harmonic interbond coupling between the hydrogens of the methylene group. Also, the off-diagonal elements include the Fermi resonance of the stretch with the overtones of the bend. The vibrational dependence on the interaction parameter k_{sbb} is expressed by[42]

$$\langle n_i,b|H/hc|n_i-1,b+2\rangle = k_{sbb}[n_i(b + 1)(b + 2)/8]^{1/2} \quad (5)$$

ω_{C-H} and x_{C-H} were retrieved from the Birge−Sponer plot of $\Delta E/V$ versus V, according to the expression[37]

$$\Delta E = \omega_{C-H}V + x_{C-H}V^2 \quad (6)$$

while considering the positions of the peaks that carry most of the intensity within the manifolds $V = 3-5$. The linear fit resulted in $\omega_{C-H} = 3072.7\ cm^{-1}$ and $x_{C-H} = -59.0\ cm^{-1}$. For δ_{C-H} we used the ν_2 bend fundamental, $1435.0\ cm^{-1}$,[35] without taking into account the other two bends (ν_5 and ν_8), which are of different symmetry and at lower energies. The rest of the LM parameters, given in cm^{-1}, were taken from refs 42 and 43 and are $\lambda^{HH} = -27.8$, $x_{bb} = -5.5$, $x_{sb} = -19.5$, and $k_{sbb} = 75.2$. The eigenvalues obtained with these parameters, after diagonalization of the matrixes, were close to those of the observed peaks. However, a better agreement was reached after the last three parameters were fitted to the measured peaks in the $V = 4$ and 5 manifolds. The fitting was only on the three parameters due to the limited number of features in the corresponding energetic regions. The resulting values after the optimization are $x_{bb} = -4.4\ cm^{-1}$, $x_{sb} = -31.0\ cm^{-1}$, and $k_{sbb} = 89.0\ cm^{-1}$, and the eigenvalues are given by the sticks of Figure 1b,c. The diagonalization of the matrixes also yielded the corresponding eigenvectors, and the heights of the sticks represent the calculated contributions from the $\{\langle v,0,0|\}$ states,[44] which indicate the coupling of the C−H LM stretching states with the rest of the C−H stretch−bend manifold. The states in the $V = 4$ and 5 manifolds are related to contributions of pure stretch and combinations of stretch and bend, whereas the main peaks correspond to a higher fraction of the former.

It is worth noting that the peaks observed in our PA spectra are narrower and shifted relative to those of the overtone spectra of liquid dichloromethane,[37] which were also analyzed by an

LM model. Furthermore, the jet-cooled action spectra revealed even narrower features than the room-temperature PA spectra due to reduction of the inhomogeneous structure.

The observed splittings imply that if energy were initially deposited into the CH stretching state under coherent excitation, the probability of finding the system in the initially excited CH would oscillate between the zero-order states with periods of $\tau = 1/c\Delta\bar{\nu}$, where $\Delta\bar{\nu}$ values are the splittings of the eigenstates (cm^{-1}).[45] The spectral splitting between the features is between 70 and 80 cm^{-1} for the $V = 3-5$ manifolds, implying oscillation periods of about 0.48−0.42 ps or redistribution times of 0.24−0.21 ps. These times are between those of $CHFCl_2$, CHF_2Cl, $CHCl_3$, and CHF_3 molecules and CH_3CF_2Cl and CH_3CFCl_2 ethane derivatives excited to the second and third overtones.[25,46] In parents with an isolated C−H chromophore the energy redistribution between C−H stretches and bends takes less than 0.1 ps mostly and in the extreme case less than 0.2 ps, while in the methyl-containing compounds it takes 0.25−0.65 ps. This behavior indicates that the mixing of stretches and bends via Fermi resonances leads to somewhat different redistribution times, where that for the molecule containing methylene is between those for molecules with an isolated C−H group or a methyl group. This energy redistribution is followed then by flow to the rest of the molecule, which is evident from the increased yield of both ground and spin−orbit-excited chlorine photofragments.

(b) Dynamics on the Upper PESs. The dynamics on the upper PESs is untangled from the branching into Cl and Cl* photoproducts and their TOF profiles. The Cl*/Cl branching ratios were determined by taking into account the areas of the Gaussian-fitted Doppler profiles and the scaling factors of the corresponding REMPI transitions.[33] The ratios were found to be almost identical, i.e., 0.55 ± 0.12, 0.52 ± 0.11, and 0.53 ± 0.12 for $\nu_{C-H} = 3-5$, respectively. These findings show that for all initial excitations the Cl* atoms are less abundant than the Cl atoms. Nevertheless, the Cl*/Cl branching ratios are significantly higher than those found by Matsumi et al.,[10] 0.25 ± 0.05 or actually the rescaled value of 0.34 ± 0.07 (after consideration of the latest ionization efficiencies for the Cl and Cl* REMPI transitions[47]), and by Tiemann et al.,[7] 0.33 ± 0.03, in the 193 photodissociation of vibrationless ground-state CH_2Cl_2. It should be noticed that the combined energies of ~51180, 53855, and 56343 cm^{-1}, used in the VMP of CH_2Cl_2 initially excited to $\nu_{C-H} = 3-5$, respectively, are below and above the energy of the 193 nm photons, 51813 cm^{-1}. Therefore, it seems unlikely that the energy difference is the cause of the branching alteration in VMP relative to that in the vibrationless ground-state CH_2Cl_2. This change is rather attributed to the variation of the VMP nonadiabatic dynamics, which determines the fragment spin−orbit splitting during its departure from the molecule. It should be noted that an increase in the branching into X* as a result of internal parent excitation was observed in several species. Particularly, variation of the CF_3I temperature in a supersonic expansion affected its thermal population or initial vibrational state, which in turn impacted the branching ratio between I* and I.[21] Furthermore, an increase in the Cl*/Cl ratio was observed in VMP of chlorine-containing molecules, including CH_3Cl, CHD_2Cl, CH_3CF_2Cl, and CH_3CFCl_2.[22,25]

The production of Cl and Cl* in photolysis of vibrationally excited CH_2Cl_2 molecules was also monitored via the ion arrival profiles, displayed in Figure 2. These profiles were monitored with the polarization of the NIR laser perpendicular to the TOFMS axis and with that of the UV photolysis/probe laser parallel or perpendicular to the axis, respectively. Figure 2

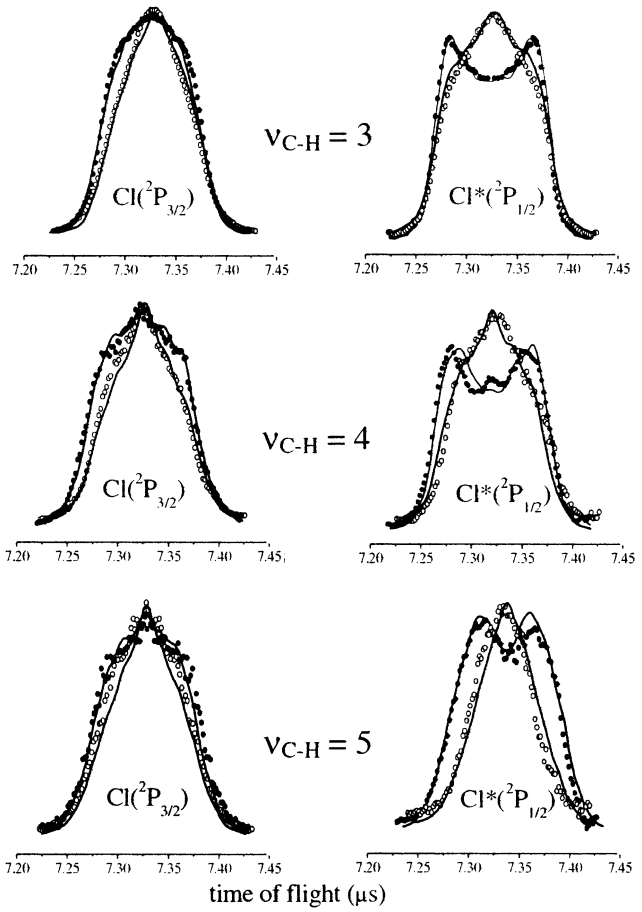

Figure 2. Arrival time profiles of $^{35}Cl(^2P_{3/2})$ and $^{35}Cl(^2P_{1/2})$ photofragments produced in the ~235 nm photolysis of CH_2Cl_2 pre-excited to $3\nu_{C-H}$, $4\nu_{C-H}$, and $5\nu_{C-H}$, where open circles and solid points are the experimental data points taken with the polarization of the UV photolysis/probe laser parallel and perpendicular, respectively, to the TOFMS axis. The polarization of the overtone excitation laser was perpendicular to the TOFMS axis. Solid lines are best fit simulations of the corresponding profiles.

displays various shapes for the Cl and Cl* photofragment profiles. Explicitly, the Cl profiles are singly peaked for both parallel and perpendicular UV laser polarizations, while those of Cl* are doubly peaked for the parallel and singly peaked for the perpendicular polarization of the UV laser. This trend is observed for all profiles, although those of $\nu_{C-H} = 5$ are noisier than those of $\nu_{C-H} = 3$ and 4, due to the smaller transition probability of the former in the vibrational excitation step. Doubly peaked profiles can occur due to instrumental or dynamical reasons. The former is ruled out since the acceleration voltages were adjusted to preclude ion-flyout of particles failing to attend the detector, due to small velocity components v_z toward the detector and large velocity components perpendicular to the detector axis. As for the second reason, it is well-known that doubly peaked profiles manifest the production of photofragments in a dissociative encounter with equal translational energies, but with velocity vectors pointing toward and opposite the flight axis. These spatially anisotropic fragments are regarded as being centered around a large average speed value, $\bar{v}$, with a relatively narrow speed distribution, $P(v)$.

Analysis of the arrival profiles was performed by considering the following. The spatial fragment distribution corresponds to $P(v,\theta) = P(v)[1+\beta(v)P_2(\cos\theta)]$, where θ is the angle between the polarization direction of the laser beam and the direction of

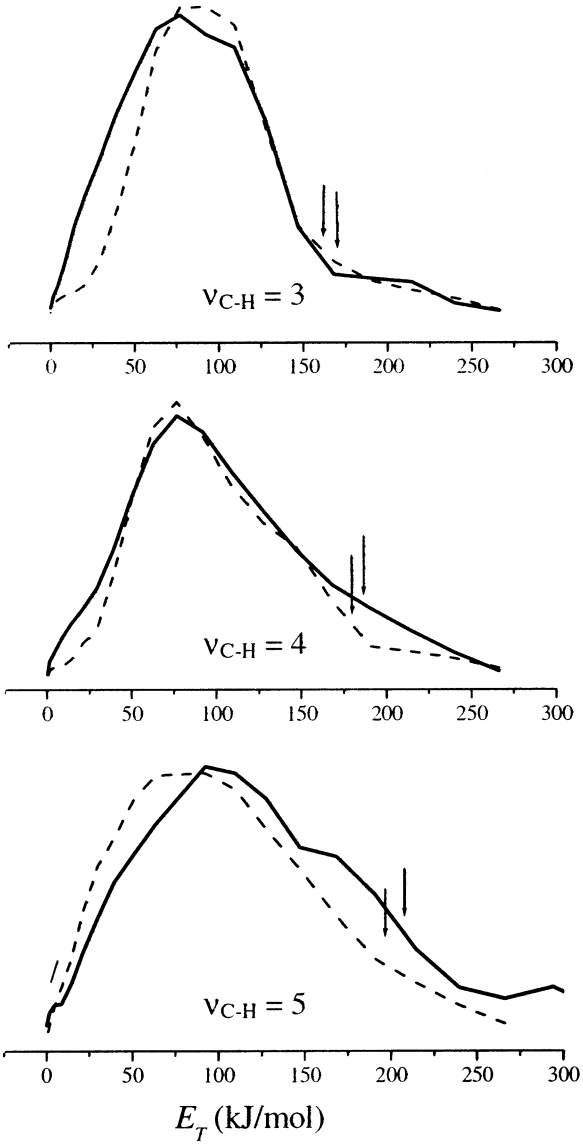

Figure 3. Energy distributions of $^{35}Cl(^2P_{3/2})$ (solid line) and $^{35}Cl(^2P_{1/2})$ (dashed line) in ~235 nm photodissociation of vibrationally excited CH_2Cl_2, $\nu_{C-H} = 3-5$. The distribution for each photofragment at a given excitation was obtained from simultaneous fitting of the parallel and perpendicular profiles. The arrows at high energies indicate the maximum possible energies calculated for release of one chlorine atom from the parent.

the flight of the photofragments, $\beta(v)$ is the velocity-dependent anisotropy parameter, ranging from -1 for a perpendicular transition to $+2$ for a pure parallel transition, and P_2 is the second Legendre polynomial, $P_2(x) = {}^1/_2(3x^2 - 1)$.[48] The β parameters and the center of mass (cm) translational energies of the Cl and Cl* photofragments were extracted via simulations of the TOF profiles by a forward convolution method, using a genetic algorithm minimizing the deviation of the simulated profile from the measured one.[30] Single velocity-independent and identical β parameters were used to simultaneously fit the profiles obtained in both polarization geometries. Nonetheless, the measured arrival profiles (solid points and open circles) were well fitted by the simulations represented by solid lines (Figure 2), resulting in the optimized translational energy distributions shown in Figure 3.

Some insight regarding the potential dissociation channels for Cl and Cl* photofragment release can be obtained by considering their energetics. The energy required for chlorine loss was estimated from the standard enthalpies of formation ($\Delta_f H°$) of the involved molecule and radicals:[49]

$$CH_2Cl_2 \xrightarrow{h\nu} CH_2Cl + Cl \ (\Delta_r H°_{298} = 334 \text{ kJ/mol}) \quad (7)$$

$$CH_2Cl_2 \xrightarrow{h\nu} CH_2 + 2Cl \ (\Delta_r H°_{298} = 728 \text{ kJ/mol}) \quad (8)$$

The reaction enthalpies, $\Delta_r H°_{298}$, for Cl* atom release via channels 7 and 8 have to be 10.6 and 21.2 kJ/mol higher. By accounting for the combined excitation energies, E_{com}, channeled into the CH_2Cl_2 molecules (Table 1) and the $\Delta_r H°_{298}$ values for loss of one or two chlorine atoms, it is possible to estimate whether reactions 7 and 8 can occur. It is clear that the combined energies employed in the experiment, even for CH_2Cl_2 initially excited to $\nu_{CH} = 5$, are insufficient to release two ground-state chlorine atoms via reaction 8. Nevertheless, the energies for CH_2Cl_2 initially excited to $\nu_{C-H} = 3-5$, exceed that required for loss of one Cl atom, leading to the maximal kinetic energies for Cl and Cl* marked by the arrows in Figure 3. Actually, these arrows should be shifted to somewhat larger values if $\Delta_r H°_0$ values are retrieved. As clearly seen from Figure 3, the energy distributions are fairly broad, centered at relatively high values with tails reaching the maximum energies of the Cl photofragments. This behavior might be indicative of a dissociation process occurring on a repulsive PES′ as also suggested by the broad and unstructured first absorption band of CH_2Cl_2.[32]

TABLE 1: Combined Excitation Energies, E_{com}, Available Fragment Energies, E_{avl}, Mean Translational Energies of the CH_2Cl and Cl Fragment Pair, $\langle E_T \rangle$, Fraction of Translational Energy Disposal, f_T, and Anisotropy Parameters, β, in ~235 nm Photodissociation of Vibrationally Excited CH_2Cl_2[a]

CH_2Cl_2		E_{com}	E_{avl}	$\langle E_T \rangle$	f_T	β
$\nu_{C-H} = 3$	Cl	612	278	147	0.53	0.14 ± 0.04
	Cl*		267	152	0.57	0.37 ± 0.08
$\nu_{C-H} = 4$	Cl	645	311	150	0.48	0.22 ± 0.03
	Cl*		300	171	0.57	0.48 ± 0.05
$\nu_{C-H} = 5$	Cl	675	341	168	0.49	0.22 ± 0.11
	Cl*		330	160	0.48	0.60 ± 0.12

[a] All energies are in kJ/mol.

In addition, the translational energy distributions obtained in VMP of CH_2Cl_2 allowed retrieval of the average translational energy $\langle E_T \rangle$ of the $CH_2Cl + Cl$ fragment pair and the fraction of translational energy disposal, $f_T = \langle E_T \rangle / E_{avl}$, which are given in Table 1. It is seen that the f_T values observed in 235 nm photodissociation of CH_2Cl_2, $\nu_{C-H} = 3-5$, are close to 0.5, implying a rather high kinetic energy release occurring in this photodissociation process. These values are comparable to those measured in photodissociation of vibrationally excited $CHFCl_2$ and CH_3CFCl_2.[30] They are also quite close to those measured by photofragment translational spectroscopy (PTS) in the 193 nm photolysis of vibrationless ground-state chloromethanes ($CHFCl_2$, $CHCl_3$, CF_2Cl_2, and $CFCl_3$) releasing Cl photofragments, which were in the range of 0.41−0.50,[16,50] but differ from that measured in 193 nm photodissociation of CH_2Cl_2 ($f_T = 0.24$) where the Cl atoms were probed by REMPI.[10] Huber and co-workers[16] pointed out that their measured translational energy distribution, $P(E_T)$, for CH_3Cl significantly differs from that obtained in ref 10. Using the argument that PTS provides the kinetic energy directly and accurately, Huber and co-workers[16] stated that the reported translational energy distribution of ref 10 was in error. At any rate, the VMP and PTS studies point to a rather high kinetic energy release, which is attributed to a direct dissociation process on a repulsive surface.

Further information regarding the bond cleavage mechanism is obtained from the determined β parameters. The magnitude and sign of β are related to the orientation of the transition dipole moment, $\boldsymbol{\mu}$, in the parent molecule, the symmetry of the involved PES′, and the excited-state lifetime. The β parameters evaluated from our experimental data for $\nu_{C-H} = 3-5$ were in the range of 0.14 ± 0.04 to 0.22 ± 0.11 for Cl and 0.37 ± 0.08 to 0.60 ± 0.12 for Cl*, where the errors were calculated from the scattering of the 10 "best" β parameters obtained from the above-mentioned simulations. Although CH_2Cl_2 is of C_{2v} symmetry, it is anticipated that the initial C−H vibrational excitation and the energy redistribution impact the geometry, distorting it and reducing its symmetry to C_s. This symmetry facilitates transitions from the vibrationally excited state of the A′ ground state to repulsive states of either A′ or A″ symmetry.

For CH_2Cl_2, the observed positive β values suggest that $\boldsymbol{\mu}$ is parallel to the line linking the two chlorine atoms and perpendicular to the CH_2 plane, matching an A″ ← A′ electronic transition. Considering the initial upper state geometry, with a Cl−C−Cl bond angle of 112°, it is implied that the theoretical limit of β for this transition should be ∼1.1. However, even though the observed β parameters for Cl and Cl* photofragments were positive, they were considerably smaller than the estimated limiting values, reflecting a partial loss of anisotropy. This loss could be due to either rotational motion during slow dissociation or some dynamical factor. Considering the above observations, the former is unlikely given that upper repulsive PESs are accessed, the promptness of the dissociation, and the large fragment translational energy. Therefore, it is suggested that a dynamical factor leads to reduction of the β parameters via some contribution of an A′ ← A′ electronic transition, reaching a β value of -1 in the limit of prompt dissociation. Thus, the positive measured β parameters of both photofragments might point toward production of both Cl and Cl* as a result of simultaneous absorption to both A′ and A″ states followed by nonadiabatic curve crossing. Since the β parameter of Cl* is larger than that of Cl, it is anticipated that the contribution of the A″ state to the production of the former is more effective and increases with the combined energy.

Conclusions

The intramolecular dynamics of dichloromethane was studied via ∼235 nm photodissociation of pre-excited CH_2Cl_2 molecules. The action and PA spectra of the $\nu_{C-H} = 3-5$ regions of CH_2Cl_2 exhibit a multiple-peak structure corresponding in terms of NM and LM models to C−H stretch overtones and combinations of C−H stretches and bends. The splittings between the features reflect subpicosecond redistribution times between the stretch−bend states, which are between those encountered for molecules with isolated C−H and methyl groups. The energy flow from the C−H to the C−Cl bond is also evident from the increased ground and spin−orbit-excited chlorine yield. The dissociation is rapid, resulting in the favored ground state over spin−orbit-excited Cl. The Cl*/Cl branching ratio in the VMP is higher than that obtained in the direct, almost isoenergetic, 193 nm photodissociation of CH_2Cl_2 and is suggestive of dynamics proceeding more nonadiabatically in the former. The nonadiabaticity of the process is also supported by the measured anisotropy parameters. These parameters are lower than the limiting values of a pure A″ ← A′ transition, indicating also involvement of A′ states, which nonadiabatically interact to release Cl and Cl*.

Acknowledgment. This paper is dedicated to the memory of Richard Bersohn whose creative experimental and theoretical research inspired generations of researchers in the field of molecular dynamics.The present research was supported by Grant No. 99-00044 from the United States-Israel Binational Foundation (BSF), by the German-Israeli Foundation (GIF) under Grant No. I 0537-098.05/97, and by the James Franck Binational German-Israeli Program in Laser-Matter Interaction. We thank Professor Paul J. Dagdigian for useful discussions.

References and Notes

(1) McFarland, M.; Kaye, J. *Photochem. Photobiol*. **1992**, *55*, 911.
(2) Kawasaki, M.; Suto, K.; Sato, Y.; Matsumi, Y.; Bersohn, R. *J. Phys. Chem*. **1996**, *100*, 19853.
(3) Shapiro, M. *J. Phys. Chem*. **1986**, *90*, 3644. Shapiro, M.; Bersohn, R. *J. Chem. Phys.* **1980**, *73*, 3810.
(4) Yabushita, S.; Morokuma, K. *Chem. Phys. Lett*. **1988**, *153*, 517. Amatatsu, Y.; Morokuma, K.; Yabushita, S. *J. Chem. Phys*. **1991**, *94*, 4858.
(5) Guo, H. *J. Chem. Phys*. **1992**, *96*, 2731. Xie, D.; Guo, H.; Amatatsu, Y.; Kosloff, R. *J. Phys. Chem. A* **2000**, *104*, 1009.
(6) Riley, S. J.; Wilson, K. R. *Faraday Discuss. Chem. Soc*. **1972**, *53*, 132.
(7) Tiemann, E.; Kanamori, H.; Hirota, E. *J. Chem. Phys*. **1988**, *88*, 2457.
(8) Continetti, R. E.; Balko, B. A.; Lee, Y. T. *J. Chem. Phys*. **1988**, *89*, 3383.
(9) Loo, R. O.; Haerri, H.-P.; Hall, G. E.; Houston, P. L. *J. Chem. Phys*. **1989**, *90*, 4222.
(10) Matsumi, Y.; Tonokura, K.; Kawasaki, M.; Inoue, G.; Satyapal, S.; Bersohn, R. *J. Chem. Phys*. **1992**, *97*, 5261; **1991**, *94*, 2669.
(11) Hess, W. P.; Chandler, D. W.; Thoman, J. W. *Chem. Phys*. **1992**, *163*, 277.
(12) Eppink, A. T. J. B.; Parker, D. H. *J. Chem. Phys*. **1999**, *110*, 832.
(13) Underwood, J. G.; Powis, I. *Phys. Chem. Chem. Phys*. **2000**, *2*, 747.
(14) van den Brom, A. J.; Lipciuc, M. L.; Janssen, M. H. M. *Chem. Phys. Lett*. **2003**, *368*, 324.
(15) Melchior, A.; Bar, I.; Rosenwaks, S. *J. Chem. Phys.* **1997**, *107*, 8476. Melchior, A.; Knupfer, P.; Bar, I.; Rosenwaks, S.; Laurent, T.; Volpp, H. R.; Wolfrum, J. *J. Phys. Chem*. **1996**, *100*, 13375.
(16) Scheld, H. A.; Furlan, A.; Huber, J. R. *Chem. Phys. Lett*. **2000**, *326*, 366. Bergmann, K.; Carter, R. T.; Hall, G. E.; Huber, J. R. *J. Chem. Phys*. **1998**, *109*, 474. Furlan, A.; Gejo, T.; Huber, J. R. *J. Phys. Chem*. **1996**, *100*, 7956. Yang, X. F.; Felder, P.; Huber, J. R. *Chem. Phys.* **1994**, *189*, 127. Baum, G.; Huber, J. R. *Chem. Phys. Lett.* **1993**, *213*, 427. Baum, G.; Huber, J. R. *Chem. Phys. Lett*. **1993**, *203*, 261.
(17) Zou, P.; McGivern, W. S.; North, S. W. *Phys. Chem. Chem. Phys*. **2000**, *2*, 3785. McGivern, W. S.; Li, R.; Zou, P.; North, S. W. *J. Chem. Phys.* **1999**, *111*, 5771.
(18) Park, M. S.; Kim, T. K.; Lee, S. H.; Jung, K. H.; Volpp, H. R.; Wolfrum, J. *J. Phys. Chem. A* **2001**, *105*, 5606. Brownsword, R. A.; Schmiechen, P.; Volpp, H. R.; Upadhyaya, H. P.; Jung, Y. J.; Jung, K. H. *J. Chem. Phys*. **1999**, *110*, 11823.
(19) Xu, H.; Guo, Y.; Liu, S.; Ma, X.; Dai, D.; Sha, G. *J. Chem. Phys.* **2002**, *117*, 5722.
(20) Rozgonyi, T.; Gonzalez, L. *J. Phys. Chem. A* **2002**, *106*, 1. Kroner, D.; Shibl, M. F.; Gonzalez, L. *Chem. Phys. Lett*. **2003**, *372*, 242.
(21) Person M. D.; Kash, P. W.; Butler L. J. *J. Chem. Phys.* **1991**, *94*, 2557.
(22) Tao, C.; Dagdigian, P. J. *Chem. Phys. Lett*. **2001**, *350*, 63. Lambert, H. M.; Dagdigian, P. J. *J. Chem. Phys.* **1998**, *109*, 7810. Lambert, H. M.; P. J. Dagdigian, *Chem. Phys. Lett.* **1997**, *275*, 499.
(23) Crim, F. F. *J. Phys. Chem*. **1996**, *100*, 12725.
(24) Bar, I.; Rosenwaks, S. *Int. Rev. Phys. Chem*. **2001**, *20*, 711.
(25) Dorfman, G.; Melchior, A.; Rosenwaks, S.; Bar, I. *J. Phys. Chem. A* **2002**, *106*, 8285. Melchior, A.; Chen, X.; Bar, I.; Rosenwaks, S. *J. Chem. Phys.* **2000**, *112*, 10787. Melchior, A.; Chen, X.; Bar, I.; Rosenwaks, S. *Chem. Phys. Lett*. **1999**, *315*, 421.
(26) Lehmann, K. K.; Scoles, G.; Pate, B. H. *Annu. Rev. Phys. Chem*. **1994**, *45*, 241.
(27) Nesbitt, D. J.; Field, R. W. *J. Phys. Chem.* **1996**, *100*, 12735 and references therein.
(28) Callegari, A.; Rizzo, T. R. *Chem. Soc. Rev.* **2001**, *30*, 214.
(29) Marom, R.; Golan, A.; Rosenwaks, S.; Bar, I. *Chem. Phys. Lett*. **2003**, *378*, 305.
(30) Chen, X.; Marom, R.; Rosenwaks, S.; Bar, I.; Einfeld, T.; Maul, C.; Gericke, K. H. *J. Chem. Phys*. **2001**, *114*, 9033. Einfeld, T.; Maul, C.; Gericke, K. H.; Marom, R.; Rosenwaks, S.; Bar, I. *J. Chem. Phys*. **2001**, *115*, 6401.
(31) Chen, X.; Ganot, Y.; Bar, I.; Rosenwaks, S. *J. Chem. Phys*. **2000**, *113*, 5134.
(32) Hubrich, C.; Stuhl, F. *J. Photochem*. **1980**, *12*, 93.

(33) Regan, P. M.; Langford, S. R.; Ascenzi, D.; Cook, P. A.; Orr-Ewing, A. J.; Ashfold, M. N. R. *Phys. Chem. Chem. Phys.* **1999**, *1*, 3247.

(34) Rothman, L. S.; Rinsland, C. P.; Goldman, A.; Massie, S. T.; Edwards, D. P.; Flaud, J.-M.; Perrin, A.; Camy-Peyret, C.; Dana, V.; Mandin, J.-Y.; Schroeder, J.; McCann, A.; Gamache, R. R.; Wattson, R. B.; Yoshino, K.; Chance, K.; Jucks, K.; Brown, L. R.; Nemtchinov, V.; Varanasi, P. *The 1996 HITRAN Molecular Spectroscopic Database and HAWKS (HITRAN Atmospheric Workstation)*, Atomic and Molecular Physics Division, Harvard−Smithsonian Center of Astrophysics.

(35) Duncan, J. L.; Nivellini, G. D.; Tullini, F. *J. Mol. Spectrosc.* **1986**, *118*, 145.

(36) Schharschmidt, V. K.; Gotzl, G. *Z. Phys. Chem. (Leipzig)* **1987**, *268*, S1105.

(37) Mortensen, O. S.; Henry, B. R.; Mohammadi, M. A. *J. Chem. Phys.* **1981**, *75*, 4800. Ahmed, M. K.; Henry, B. R. *J. Phys. Chem.* **1986**, *90*, 1993.

(38) Halonen, L. *J. Chem. Phys.* **1988**, *88*, 7599.

(39) Herzberg G. *Molecular Spectra and Molecular Structure. II Infrared and Raman Spectra of Polyatomic Molecules*; Van Nostrand Reinhold Co.: New York, 1945.

(40) Child, M. S.; Halonen, L. *Adv. Chem. Phys.* **1984**, *57*, 1.

(41) Mills, I. M.; Robiette, A.G. *Mol. Phys.* **1985**, *56*, 743.

(42) Duncan, J. L.; New, C. A.; Leavitt, B. *J. Chem. Phys.* **1995**, *102*, 4012.

(43) Law, M. M. *J. Chem. Phys.* **1999**, *111*, 10021.

(44) The first two quantum numbers represent the excitation between the identical two bonds of the methylene, and the third quantum number denotes the bending in the $\langle v,0,0|$ states of the LM basis. $\{\langle v,0,0|\}$ refers to the equivalent combinations of $\langle v,0,0|$ and $\langle 0,v,0|$.

(45) Boyarkin, O. V.; Settle, R. D. F.; Rizzo, T. R. *Ber. Bunsen-Ges. Phys. Chem.* **1995**, *99*, 504.

(46) Dubal, H.-R.; Quack, M. *J. Chem. Phys.* **1984**, *81*, 3779. Hippler, M.; Quack, M. *J. Chem. Phys.* **1996**, *104*, 7426

(47) Zhang, J.; Dulligan, M.; Wittig, C. *J. Chem. Phys.* **1997**, *107*, 1403.

(48) Zare, R. N. *Mol. Photochem.* **1972**, *4*, 1.

(49) Atkinson, R.; Baulch, D. L.; Cox, R. A.; Hampson, R. F., Jr.; Kerr, J. A.; Rossi, M. J.; Troe, J. *J. Phys. Chem. Ref. Data* **2000**, *29*, 167.

(50) Nachbor, M. D.; Giese, C. F.; Gentry, W. R. *J. Phys. Chem.* **1995**, *99*, 15400.